

Semi-supervised Semantic Segmentation for Remote Sensing Images via Multi-scale Uncertainty Consistency and Cross-Teacher-Student Attention

Shanwen Wang, Changrui Chen, Xin Sun, Danfeng Hong, Jungong Han

Abstract—Semi-supervised learning offers an appealing solution for remote sensing (RS) image segmentation to relieve the burden of labor-intensive pixel-level labeling. However, RS images pose unique challenges, including rich multi-scale features and high inter-class similarity. To address these problems, this paper proposes a novel semi-supervised Multi-Scale Uncertainty and Cross-Teacher-Student Attention (MUCA) model for RS image semantic segmentation tasks. Specifically, MUCA constrains the consistency among feature maps at different layers of the network by introducing a multi-scale uncertainty consistency regularization. It improves the multi-scale learning capability of semi-supervised algorithms on unlabeled data. Additionally, MUCA utilizes a Cross-Teacher-Student attention mechanism to guide the student network, guiding the student network to construct more discriminative feature representations through complementary features from the teacher network. This design effectively integrates weak and strong augmentations (WA and SA) to further boost segmentation performance. To verify the effectiveness of our model, we conduct extensive experiments on ISPRS-Potsdam and LoveDA datasets. The experimental results show the superiority of our method over state-of-the-art semi-supervised methods. Notably, our model excels in distinguishing highly similar objects, showcasing its potential for advancing semi-supervised RS image segmentation tasks.

Index Terms—Remote Sensing Images, Semi-supervised Semantic Segmentation, Deep Learning, Consistency Regularization.

I. INTRODUCTION

DEEP learning techniques on sensing images semantic segmentation [1], [2] provide promising solutions for disaster prevention [3], land-use surveillance [4], environment protection [5], and urban planning [6]. The increasing number of Earth-observation satellites makes a large amount of raw remote sensing (RS) images be continuously captured, which amplifies the advantage of deep learning methods [7]. However, it is a time-consuming and laborious task to manually label a large amount of RS data into a large number of categories with the complexity of labeling rules [8]. Therefore, semi-supervised learning draws the attention of the RS communities,

S. Wang and X. Sun are with Faculty of Data Science, City University of Macau, 999078, SAR Macao, China. C. Chen is with WMG, University of Warwick, UK. D. Hong is with the Aerospace Information Research Institute, Chinese Academy of Sciences, Beijing 100094, China, and also with the School of Electronic, Electrical and Communication Engineering, University of Chinese Academy of Sciences, Beijing 100049, China. J. Han is with Department of Automation, Tsinghua University, Beijing, China.

This work is supported by the Science and Technology Development Fund, Macao SAR No.0006/2024/RIA1 and National Natural Science Foundation of China under Project No. 61971388.

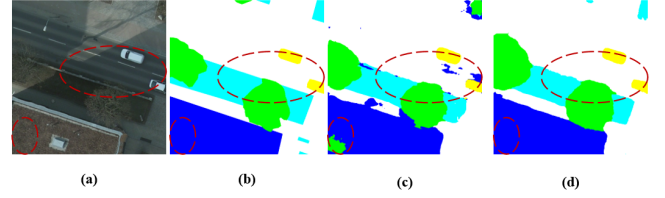


Fig. 1. (a) Image from ISPRS-Potsdam dataset. (b) Ground Truth. (c) Unimatch. (d) Ours.

because it only uses a small number of labeled samples and a large amount of unlabeled [9].

Several semi-supervised semantic segmentation methods have been conducted for natural images, which are mainly divided into teacher-student consistency [10], feature perturbation consistency [11], and self-training pseudo-labeling [12]. Self-training pseudo-labeling methods often experience performance degradation due to incorrect pseudo-labels generated in the early stages, which can lead to error propagation. Feature perturbation consistency approaches rely heavily on selecting appropriate perturbations and balanced labeled data, making them particularly sensitive to data imbalance. Among these, the teacher-student consistency framework stands out as the most stable and is especially well-suited for tasks that demand high model complexity [13]. Recent works [9], [14] have introduced semi-supervised segmentation into the field of RS image analysis, meanwhile, encountered some domain-specific problems [15], e.g., rich multi-scale information and high inter-class similarities. Such inherent domain gaps between natural and RS images pose great challenges for semi-supervised RS image segmentation.

- 1) Rich Multi-scale Information [16]: Objects on the RS image exhibit a wide range of scales, from expansive objects (e.g., Building) to small entities (e.g., Car). Moreover, objects from the same category, captured by satellites and drones with various resolutions, provide quite different features and context information.
- 2) High Inter-class Similarities [17]: Objects from different categories appear to have high visual similarity and are usually intertwined on the RS images. For example, as shown in Fig. 1(c), the boundary regions of Low vegetation, Tree, Car, and Building are misclassified with Unimatch [18].

To address the above challenges, we propose a new semi-supervised semantic segmentation model for RS images based

on Multi-Scale Uncertainty and Cross-Teacher-Student Attention (MUCA). (1) Firstly, we propose for the first time a Multi-Scale Uncertainty consistency regularization module. The module constrains the consistency among feature maps at different layers of the network model, which improves the multi-scale learning capability of semi-supervised algorithms on unlabeled data. The traditional semi-supervised algorithms perform the consistent regularization between teacher and student only at the last layer, which ignores the rich information learned in the intermediate layers from the large amount of unlabeled data. In contrast, our proposed semi-supervised method can learn efficient and rich multi-scale information from unlabeled RS images with our MSUC module. (2) Secondly, to solve the problem of high inter-class similarities, the key is to improve the feature extraction ability of the model. Therefore, we propose a Cross-Teacher-Student Attention which makes the teacher network to help the student reconstruct the outputs of the encoder. Specifically, it takes the encoder result of the student as the query and the result of the teacher as the key and value. The benefit of such cross-network attention is that deep features can be learned from both the student and teacher models. It can help segment the hard-to-distinguish categories in RS images. For instance, as shown in Fig. 1, our semi-supervised model Fig. 1 (d) can achieve more accurate segmentation results than the SOTA Unimatch method Fig. 1 (c) on RS images.

It is noteworthy that the proposed model is non-intrusive and can be easily integrated into existing semantic segmentation algorithms without changing the network structure of the model itself. Overall, the major contributions of this work can be summarized as follows:

- 1) We propose a novel semi-supervised model MUCA, specifically, to address the challenge of rich multi-scale information and high inter-class similarities in RS semantic segmentation.
- 2) To learn rich multi-scale information, MUCA introduces multi-scale uncertainty consistency regularization that constrains the consistency among feature maps at different layers of the network.
- 3) To distinguish the high inter-class similarities, MUCA utilizes a new cross-teacher-student attention to guide the student network in reconstructing discriminative encodings by the teacher.
- 4) Extensive experimental results demonstrate the efficacy of our MUCA model on the LoveDA and Potsdam datasets, compared to some SOTA methods. The results show promising achievement in RS semi-supervised segmentation tasks and highlight the significance of our contributions.

The rest of this article is organized as follows: Section II briefly introduces the related work. In Section III, our model MUCA are proposed and discussed. Section IV shows the experimental results and compares them with other SOTA methods. Section V concludes the article.

II. RELATED WORK

In recent years, the developments of deep neural networks have encouraged the emergence of a series of works on semi-

supervised semantic segmentation of RS images. This section gives a short description of recent developments in related fields.

A. RS semantic segmentation

Semantic segmentation is to segment an image into regional blocks with certain semantic meanings [19], and recognize the specific semantic category of each regional block respectively. It commonly labels the image pixel by pixel [20]–[23]. Early semantic segmentation models including FCN [24], SegNet [25], and U-Net [26], achieved remarkable performance in traditional semantic segmentation tasks. With the success of Transformers in vision in recent years, more and more semantic segmentation models are adopting the Transformers architecture [27]. Complex backgrounds as well as resolution variations are the main challenges in semantic segmentation of RS images. In RS images, large intra-class and small inter-class variations between objects make image feature characterization difficult. Workman et al. [28] argued that samples with high-resolution labels can be used to guide the training process in supervised learning using low-resolution labels. Region aggregation methods have also been used to improve the resolution of images. Quan et al. [29] utilized multi-scale edge features obtained by Differential Difference of Gaussian (DoG) methods to improve the results of edge extraction. Li et al. [30] proposed a progressive recurrent neural network to remove RS images destriping. Zhong et al. [31] proposed a transformer-based noise identification network model to help mitigate the over-segmentation phenomenon. However, semantic segmentation algorithms rely heavily on a large amount of training data, and it is difficult for these frameworks to achieve good results when labeled data is limited.

B. Semi-supervised Semantic Segmentation

Semi-supervised semantic segmentation algorithms focus on how to better utilize large amounts of unlabeled data than supervised algorithms. Most semi-supervised semantic segmentation models use a basic convolutional neural network as the backbone, and implement semi-supervised algorithms in three different strategies.

The first strategy is pseudo-labeling for self-training, which involves generating pseudo-labels for unlabeled images based on a previously trained model on labeled data. It trains the model with newly generated images with pseudo-labels [32]–[34]. The second strategy is to optimize the model by optimizing the consistent regularized loss function of feature perturbations [27], [35]–[37]. Such methods utilize data-enhancement techniques to apply perturbations directly to the input image. They force the model to predict the same labels for both original and enhanced images. Some feature-based perturbation methods add internal perturbations to the segmentation network, resulting in a modified feature [38]. UniMatch [18] took into account the nature of the semantic segmentation task and merged appropriate data augmentation into FixMatch [11], which has evolved into a concise baseline of semi-supervised semantic segmentation algorithms. The last strategy

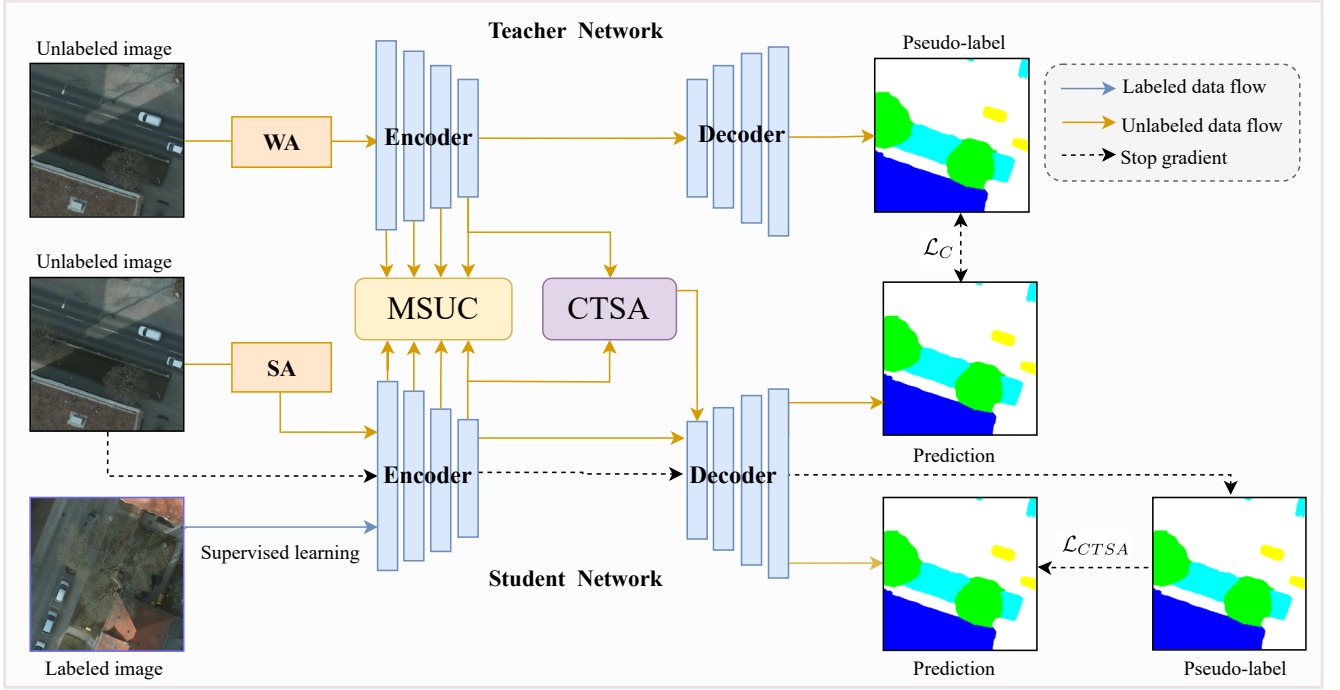


Fig. 2. Overall structure of our semi-supervised semantic segmentation model for RS images. The top and bottom sections correspond to the teacher and student networks, respectively. Blue lines indicate labeled data flow, yellow lines indicate unlabeled data flow, and dashed lines indicate data flow where gradient updating stops. The teacher network and student network interaction part contains the MSUC module and CTSA module proposed in this paper.

is teacher-student consistency [39]. The most classical method based on consistency regularization is the Mean-teacher [10]. It considers the consistency between the predictions of the student and the teacher network. The weights of the teacher network are calculated from the exponential moving average (EMA) of the weights of the student's network. Recently, a few works have applied the teacher-student consistency method to the field of semi-supervision of RS images [9].

C. Semi-Supervised Semantic Segmentation in RS Images

Semi-supervised remote sensing semantic segmentation has drawn more and more attention to make better use of the large amount of unlabeled RS image data [40]–[43]. Zhang et al. [14] proposed a new self-training mechanism for generating pseudo-labels with feature-level relationships between neighbor pixels to normalize the predictions of the adaptive model. Fang et al. [40] proposed an approximate rank-order clustering (AROC) model. This model is applied to cluster deep features, thereby generating pseudo-labels for abundant unlabeled samples. Li et al. [44] proposed a new self-supervised edge perception learning framework to mine the potential information hidden at the edge of the target. Huang et al. [9] proposed a decoupled weighted learning (DWL) framework for semi-supervised RS image segmentation. The introduced decoupled learning module separates the prediction of labeled and unlabeled data during the training process, in order to reduce the negative impact of erroneously pseudo-labeled unlabeled data on the training procedure.

These techniques and models improve the performance of semantic segmentation of RS images in the case of a

small number of labeled images. This work proposes new solutions through the viewpoint of inherent scale diversity and similarity among intra-class and inter-class to address the above challenges.

III. METHODS

This section is organized as follows: Section III-A describes the main optimization objectives, Section III-B introduces the principles of the multi-scale uncertainty consistency module, and Section III-C presents the basic principles of the cross-teacher-student attention module. The overall structure of our approach is shown in Fig. 2.

A. Main Optimization Objectives

We define $D^L = \{(x_i^l, y_i)\}_{i=1}^{N_L}$ as labeled data and $D^U = \{(x_i^u)\}_{i=1}^{N_U}$ as unlabeled. Here $x_i^l \in \mathbb{R}^{H \times W \times 3}$ denotes the labeled image, $y_i \in \mathbb{R}^{H \times W \times K}$ is the ground truth of K classes, while $x_i^u \in \mathbb{R}^{H \times W \times 3}$ denotes the unlabeled image, N_L and N_U are the amount of labeled and unlabeled images. H and W specify the height and width of the image. It is worth noting that in general N_U is much larger than N_L . For unlabeled images, weak augmentation (WA) and strong augmentation (SA) are performed to train the student and teacher networks respectively. The main loss function is:

$$\mathcal{L} = \mathcal{L}_S + \mathcal{L}_U = \frac{1}{N_L} \sum_{i=0}^{N_L} \mathcal{L}_{CE}(p_i^l, y_i) + \mathcal{L}_U, \quad (1)$$

where \mathcal{L}_S represents the loss of supervised learning with labeled data, and \mathcal{L}_U represents the loss with unlabeled data,

p_i^l is the prediction result of the labeled image x_i^l , \mathcal{L}_{CE} is the cross-entropy loss. More specifically, for \mathcal{L}_U , it consists of three parts.

$$\mathcal{L}_U = \mathcal{L}_C + \mathcal{L}_{MSUC} + \mathcal{L}_{CTSA}. \quad (2)$$

The first part \mathcal{L}_C is the basic teacher-student consistency loss function, similar to the Mean-teacher model [13]. The second part is the loss function \mathcal{L}_{MSUC} for multi-scale uncertainty consistency, and the third part \mathcal{L}_{CTSA} is related to cross-teacher-student attention, which will be introduced later.

B. Multi-Scale Uncertainty Consistency Module

Basic models of teacher-student architectures update the teacher's weights θ^t by the exponential moving average (EMA) with the student's weights θ^s . It integrates the information from different training steps. The teacher's weight θ_t^t is updated at training step t as $\theta_t^t = \alpha\theta_{t-1}^t + (1-\alpha)\theta_t^s$, where α is the EMA decay. This basic teacher-student architecture is widely used in semi-supervised networks. However, it is critical to take into account the inherent difference between RS and natural images. Objects in RS images exhibit a wide range of scales, spanning from large buildings to small vehicles, and the same object can appear at varying sizes under different resolutions. Therefore, semi-supervised learning in RS images is difficult to extract effective features. To solve this problem, we propose a Multi-Scale Uncertainty Consistency (MSUC) module for the student to progressively learn multi-scale features from reliable targets, as shown in Fig. 3. Given a batch of training images, the teacher model not only generates pseudo-labels for target prediction, but also estimates the uncertainty of each target at multiple feature levels. It optimizes the student model through multilevel consistency loss. This will motivate the model to learn different layers and sizes of features from RS images.

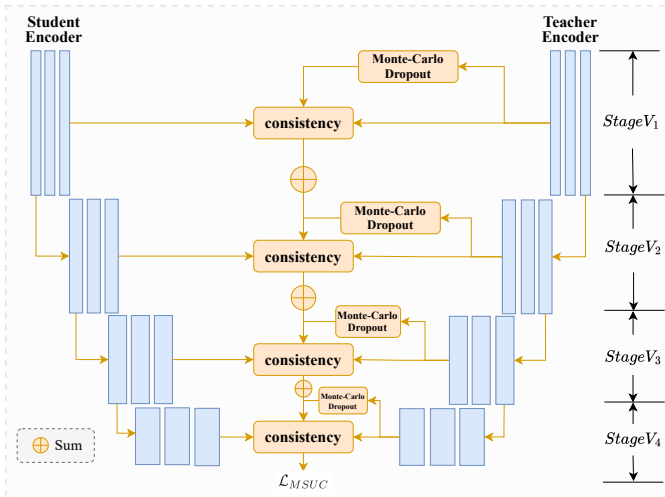


Fig. 3. MSUC model structure. Uncertainty is computed for the feature layer at each stage of the teacher and student networks, and features with high uncertainty are discarded when computing consistency regularization.

Uncertainty Estimation: We use Monte-Carlo Dropout [45] to estimate uncertainty. Monte-Carlo method can not only calculate the uncertainty between different classes but also evaluate the uncertainty in the multiple predictions of a neural network. The basic principle of Monte-Carlo Dropout is to make predictions of T times for the same sample with the same model. These T predictions are different, and their variance is calculated to compute the model uncertainty. In detail, we perform T random forward passes for the teacher model, each of which uses the random dropout and noise. Thus, for each pixel in the image, we obtain a set of softmax probability vectors: $\{p_t\}_{t=1}^T$. We choose the prediction entropy as a measure of the approximate uncertainty because it has a fixed range. Formally, the prediction entropy can be summarized as:

$$u_k = \frac{1}{T} \sum_{t=1}^T p_t^k, \quad (3)$$

$$u = - \sum_{k=1}^K u_k \log(u_k), \quad (4)$$

where p_t^k is the result of pixels of the class k in the t^{th} prediction procedure. In this way, the uncertainty of multiple predictions for the same class can be calculated. According to Eq. 3 and Eq. 4, the value u increases when the network provides completely opposite predictions many times. Moreover, Eq. 3 and Eq. 4 can also take into account the uncertainty between different classes. If the neural network gives similar predictions across multiple classes, the uncertainty value u will also increase.

Consistency Loss Functions for Multiscale Uncertainty:

To formally describe MSUC, we denote the encoded features from the four stages of the encoder as $V_i \in \mathbb{R}^{C_i H_i W_i}$, $i \in \{1, 2, 3, 4\}$, where C_i , H_i , and W_i denote the number of channels, the height, and the width of the feature maps from the i^{th} stage, as shown in Fig. 3. More specifically, V_1 is the output of the first stage with the lowest abstraction but the highest spatial resolution, and V_4 is the output of the fourth stage with the highest abstraction but the lowest spatial resolution. The final consistency loss function was computed by aligning the encoded visual features at each stage of the student model and the teacher model.

$$\mathcal{L}_{MSUC} = \sum_{i=1}^4 \frac{\sum_m \mathbb{I}(u_{i_m} < H) \mathcal{L}_\varrho(V_{i_m}^t - V_{i_m}^s)}{\sum_m \mathbb{I}(u_{i_m} < H)}, \quad (5)$$

where $V_{i_m}^t$ and $V_{i_m}^s$ are the outputs of the teacher and student encoders at the pixel m of the i^{th} stage, u_{i_m} is the uncertainty at the pixel m of the i^{th} stage, \mathbb{I} is the indicator function, and H is a threshold. \mathcal{L}_ϱ is the Huber loss function, which is formulated as follows:

$$\mathcal{L}_\varrho(V_{i_m}^t - V_{i_m}^s) = \begin{cases} \frac{1}{2} (V_{i_m}^t - V_{i_m}^s)^2 & \text{if } |V_{i_m}^t - V_{i_m}^s| \leq \varrho \\ \varrho |V_{i_m}^t - V_{i_m}^s| - \frac{1}{2} \varrho^2 & \text{otherwise} \end{cases} \quad (6)$$

where ϱ is the soft threshold for Huber loss, which is set to 1.0 in this paper.

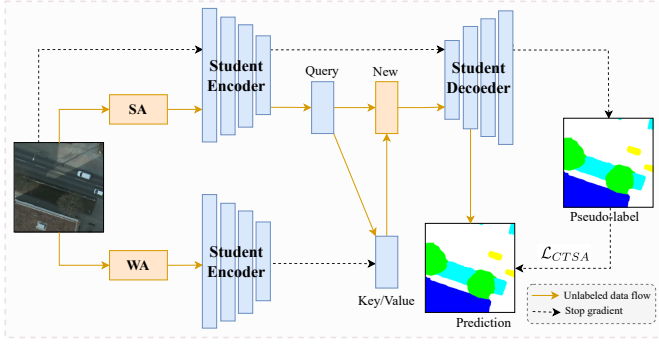


Fig. 4. CTSA model structure. An attention approach allows the teacher network to guide the student network in reconstructing the student network's encoder results.

C. Cross-Teacher-Student Attention

We propose the Cross-Teacher-Student Attention (CTSA) model, as illustrated in Fig. 4, to promote the ability of semi-supervised segmentation method for objects with high inter-class similarities.

Consistency regularization methods are based on the assumption of smoothness [46]. This means that a robust model should produce similar predictions for points and their variants with noise. In other words, a model trained with consistency methods should not be affected by different perturbations added to the data. However such semi-supervised frameworks ignore the inherent domain gap between natural and RS images. One RS image contains much richer content than one natural image, and objects of different categories are commonly intertwined. Therefore perturbations will make the RS image contain more confusing information. The features learned by the neural network from different perturbed RS images may lead to some outliers as pseudo-annotations, misleading the training of the model on unannotated data.

To address this problem, we use the features extracted by the student and teacher networks via different perturbations to reconstruct the features of the unlabeled data. We use the encoder result of the student as *query* and the encoder result of the teacher as *key* and *value*. The teacher guides the reconstruction of the encoder of the student, as shown in Fig. 4. Specifically, we calculate the similarity between each channel of the unlabeled features of the student and teacher networks. The channels with higher similarity are more important in reconstructing the unlabeled features.

More importantly, the new features constructed through CTSA effectively integrate the advantages of the teacher and student network encoders. Specifically, the SA data fed into the student encoder provides the original features which are diverse and rich. Meanwhile, the teacher encoder, receiving WA data, reconstructs another set of smooth and stable features. The decoder is trained using features generated from strongly supervised data along with features reconstructed by CTSA, resulting in better optimization outcomes. Particularly in the early stages of semi-supervised learning, where training instability and low-quality pseudo-labels often hinder efficient convergence, the teacher network encoder provides more easily learnable features for the student network decoder. This

improves the model's stability, mitigates training fluctuations, accelerates convergence, and enhances training efficiency.

We further clarify the CTSA formulation as follows. Given the student and teacher characteristics V_4^s and V_4^t after the fourth stage of the encoder, we set V_4^s as *query*, V_4^t as *key* and *value*, in a multi-head manner:

$$F^{V_4^s} = \text{flatten}(V_4^s), F^{V_4^t} = \text{flatten}(V_4^t), \quad (7)$$

$$q = F^{V_4^s} w_q, k = F^{V_4^t} w_k, v = F^{V_4^t} w_v, \quad (8)$$

where $w_q, w_k, w_v \in \mathbb{R}^{C \times 2C}$ are the transformer weights, $F^{V_4^s}, F^{V_4^t} \in \mathbb{R}^{C \times d}$, d is the number of patches and C is the channel dimension. The CTSA is defined as:

$$V_{out} = \phi[\psi(q^T k)v^T w_{out}], \quad (9)$$

where ψ denotes instance normalization and ϕ is softmax function. V_{out} is fed into the decoder to get the final predicted value of the CTSA module as described below:

$$p^u = \text{Decoder}(V_{out}). \quad (10)$$

The loss function for the CTSA module is calculated as Eq. 20, where \hat{y}_i is the generated pseudo-label from unlabeled data.

$$\mathcal{L}_{CTSA} = \frac{1}{N_U} \sum_{i=0}^{N_U} \mathcal{L}_{CE}(p_i^u, \hat{y}_i), \quad (11)$$

Algorithm 1 Training process of MUCA

Input:

$$D_U^e = \{(x_i^u)\}_{i=1}^{N_U^e}, D_L^e = \{(x_i^l, y_i)\}_{i=1}^{N_L^e}$$

Output:

Θ : optimal model parameters

1: **while** until converge:

2: **for** x_i^l, x_i^u in D_L^e, D_U^e :

3: $\mathcal{L}_S = CE(\text{model}_s(x_i^l), y_i)$

6: $W_x_i^u = \text{WeakAugment}(x_i^u)$

7: $S_x_i^u = \text{StrongAugment}(x_i^u)$

8: $V^s, Enc_s, Pre_s = \text{model}_s(S_x_i^u)$

9: $V^t, Enc_t, Pseudo_t = \text{model}_t(W_x_i^u)$

10: $\mathcal{L}_C = \text{Huber}(Pre_s, Pseudo_t)$

11: **for** j in $[1:4]$:

12: Calculate uncertainty u via Eq. 4

13: **if** $u < H$:

14: Calculate \mathcal{L}_{MSUC} of j stage via Eq. 5

15: $\mathcal{L}_{MSUC} += \mathcal{L}_{MSUC}$

16: **end for**

17: $Pseudo_s = \text{model}_s(x_i^u).detach()$

18: $Enc_{new} = \text{model}_s_d(CTSA(Enc_s, Enc_t))$

19: $\mathcal{L}_{CTSA} = CE(Enc_{new}, Pseudo_s)$

20: $\mathcal{L}_U = \mathcal{L}_C + \mathcal{L}_{CTSA} + \mathcal{L}_{MSUC}$

21: **end for**

22: $\mathcal{L} = \mathcal{L}_S + \mathcal{L}_U$

23: Back propagating the \mathcal{L} and update Θ

24: Mark the current model checkpoint and use it to predict pseudo labels of unlabeled images

25: Save the best checkpoint Θ

26: **return** Θ

Algorithm 1 gives the core pseudo-code for the training process of MUCA on the unlabeled data. D_U^e and D_L^e are the unsupervised and supervised datasets for one epoch. N_U^e and N_L^e are number of images in D_U^e and D_L^e . $model_s$ and $model_t$ denote the student and teacher models. $model_s_d$ is the decoder of the student model. V^s and V^t are the feature maps extracted by the encoders of the student network and the teacher network. Enc_s and Enc_t are the output results of the student network and teacher network encoders. Pre_s represents the final prediction of the student network. $Pseudo_t$ represents the pseudo-labels generated by the teacher network, and $Pseudo_s$ represents the pseudo-labels generated by the student network. CE is the Cross-Entropy loss function, and $Huber$ is the Huber loss function.

IV. EXPERIMENT

In this section, we conduct experiments on semi-supervised semantic segmentation of RS images to evaluate the proposed MUCA model. We first perform ablation studies on MUCA to validate the effectiveness of the proposed modules. Then, we conducted comparative experiments to compare MUCA with several SOTA models. Our code is released at <https://github.com/wangshanwen001/RS-MUCA>.

A. RS Dataset

LoveDA: The LoveDA RS dataset [47] consists of 5987 images and 166,768 annotated objects from three different cities. Each image is 1024×1024 with a spatial resolution of 0.3 meters. The dataset has seven segmentable classes, such as Building, Road, Water, Barren, Forest, Agriculture, and Background. Due to the memory limitations of the GPU, each image in the LoveDA dataset is resized and cropped to 512×512 , producing a total of 16,764 cropped images for subsequent deep learning training. During training, we divide the dataset into training set, validation set, and test set by 6:2:2.

ISPRS-Potsdam: The ISPRS-Potsdam RS dataset is provided to facilitate research on RS images semantic segmentation [48]. This dataset has a resolution of 0.05 meters and consists of 38 super-large satellite RS images of 6000×6000 size. There are six segmentable classes in the dataset including Impervious surfaces, Building, Low vegetation, Tree, Car, and Background. To facilitate the training procedure, we crop the original image into 512×512 and the number of cropped images is 5472. The dataset is divided into training, validation and test sets by 6:2:2.

B. Data Augmentation and Experiment Details

We first augmentation the labeled images via geometric transformations (i.e., image scaling, horizontal flipping, vertical flipping and length and width warping) and Gaussian blurring. The weak augmentation used for unlabeled images is geometric augmentation, and strong augmentation is done by methods such as CutMix [49].

The experiments are conducted on A6000 (48G) with Python-3.8.10, Pytorch-1.13.0, and Cuda v11.7. The optimization algorithm is stochastic gradient descent with an initial

learning rate 0.007. The learning rate is updated on each epoch, the weight decay is set to 0.0001, and the minimum learning rate is set to 0.00007. Then, we train the semi-supervised segmentation model using 1%, 5% and 10% of the labeled images and the remaining unlabeled images.

C. Evaluation metrics

Most of the popular semantic segmentation metrics are employed to comprehensively evaluate the performance, e.g., intersection and concurrency ratio (IoU), F1-Score (F1), and Cohen's Kappa as show below:

$$IoU = \frac{TP}{TP + FN + FP}, \quad (12)$$

$$Recall = \frac{TP}{TP + FN}, \quad (13)$$

$$Precision = \frac{TP}{TP + FP}, \quad (14)$$

$$F1 = \frac{2 \times Recall \times Precision}{Recall + Precision}, \quad (15)$$

$$OA = \frac{TP + TN}{TP + TN + FP + FN}, \quad (16)$$

$$PRE = \frac{(TP + FN)(TP + FP) + (TN + FN)(TN + FP)}{(TP + TN + FP + FN)^2}, \quad (17)$$

$$Kappa = \frac{OA - PRE}{1 - PRE}, \quad (18)$$

where TP is the number of correctly predicted positive pixels, TN is the number of correctly predicted negative pixels, FP is the number of incorrectly predicted positive pixels, and FN is the number of incorrectly predicted negative pixels. In our experiments we average IoU and $F1$ across all classes, so the final experimental metrics also include mean IoU ($mIoU$) and mean $F1$ ($mF1$). Then, $mIoU$ and $mF1$ is calculated as follows:

$$mIoU = \frac{\sum_{i=1}^K IoU_i}{K}, \quad (19)$$

$$mF1 = \frac{\sum_{i=1}^K F1_i}{K}, \quad (20)$$

where IoU_i means the IoU of the i^{th} class and K is the number of classes.

D. Ablation study

Ablation of components: We ablate each component step by step to investigate their performance. It is worth noting that we also evaluate the multi-scale consistency loss function of MSUC module without uncertainty, which is denoted as NoUC. Differing from the MSUC module, NoUC only uses standard consistency regularization to compute the loss for each hierarchical feature map. The ablation studies are conducted on the ISPRS-Potsdam dataset with labeled data ratio of 5%. The baseline is the supervised model with 5% labeled

TABLE I
ABLATION STUDY ON THE EFFECTIVENESS OF COMPONENTS.

NoUC	MSUC	CTSA	mIoU (5%)
			72.01
✓			73.14
	✓		73.95
		✓	73.80
	✓	✓	74.62

data. The semantic segmentation model used in this subsection is SegFormer-B2.

The experimental results are shown in Table I. Compared to the baseline, the NoUC module improves the $mIoU$ by 1.13%. The MSUC improves the $mIoU$ by 0.81% compared to the NoUC and 1.94% to the baseline. It demonstrates that computational uncertainty enables the student network to exclude uncertain information and learn from meaningful and reliable objects. The $mIoU$ of the CTSA module improves by 1.81% to the baseline, demonstrating that the CTSA attention mechanism extracts distinguishable features. Finally, the model improves by 2.61% over the baseline.

TABLE II
THE IMPACT OF CTSA MODULE IN THE TEST STAGE.

Stage	CTSA	mIoU (5%)
Test	✓	73.80 73.87

Should we integrate the CTSA module in the test stage?

The CTSA module requires both teacher-student networks to complete the attention. However, generally speaking, we only save one final checkpoint file. In this study, we save both the teacher and student checkpoint files in each epoch. We then investigate the influences of CTSA on the $mIoU$ in the testing stage. As shown in Table II, the impact of the CTSA module is almost negligible in the testing phase. The double disk consumption and limited performance improvement make us abandon the CTSA module in the testing phase.

TABLE III
ANALYSIS OF MULTI-LEVEL FEATURE MAPS OF MSUC MODULE.

V_1	V_2	V_3	V_4	mIoU (5%)
				72.01
✓				72.41
	✓			72.55
		✓		72.76
			✓	72.96

Analysis of multi-level feature maps of MSUC module: MSUC encodes visual features from the four stages of the encoder, i.e., $V_i \in \mathbb{R}^{C_i H_i W_i}$, $i \in \{1, 2, 3, 4\}$. Therefore, it is critical to explore the impact of multi-level (i.e., low to high) deep features on our MSUC. From Table III, we can see that the deep MSUC feature V_4 achieves greater improvement than the other low-level features, while the lowest feature V_1 makes the worst mIoU. The reason is that the deep features have a rich representation of information.

TABLE IV
ANALYSIS OF DEEP AND LOW FEATURES FUSION FOR MSUC MODULE.

V_1	V_2	V_3	V_4	mIoU (5%)
				72.01
			✓	72.96
		✓	✓	73.42
	✓	✓	✓	73.66
✓	✓	✓	✓	73.95

Analysis of features fusion for MSUC module.: We fuse deep and low features stage by stage for the MSUC module. Specifically, we firstly employ the deep feature V_4 alone, and then gradually add all the other level features. Table IV shows the results of these different combinations. From the results, we observe that the mIoU gradually increases as lower level features are added stage by stage. This is because low features contain more local information, which can effectively compensate deep features. The fusion of deep and low features improves the consistency of the model at different layers and resolutions, and optimizes the semantic segmentation results of RS images.

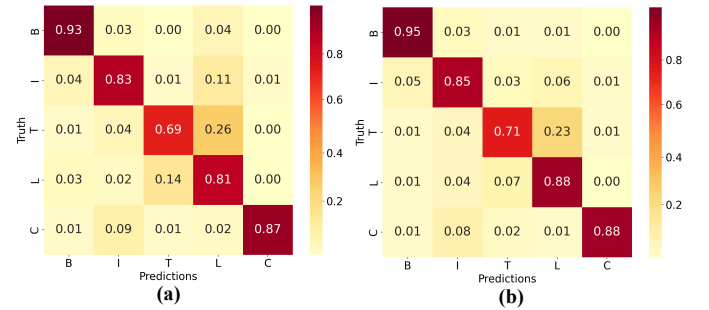


Fig. 5. Visualization confusion matrix of model without MUCA (a) and with MUCA (b). Car (C), Low vegetation (V), Tree (T), Impervious surfaces (S), and Building (B).

Confusion Matrix Visualization: We visualized the confusion matrices of the Potsdam dataset at labeled data ratio of 5%, as shown in Fig. 5. It intuitively demonstrates the improvement of the semi-supervised semantic segmentation with MUCA. We perform a row normalization on the confusion matrix, where the redder of the color the closer to the truth. We can see that the introduced MUCA significantly improves the ability to distinguish hard-to-differentiate classes such as Low vegetation and Tree.

E. Comparison with SOTA methods on RS Datasets

This section conducts experiments on ISPRS-Potsdam and LoveDA datasets, compared to the SOTA methods, including Mean teacher [10], CutMix [49], CCT [38], CPS [39], LSST [50], Fixmatch [11], Unimatch [18], DWL [9], and Allspark [12]. Specifically, we show the results for labeled data ratios of 1%, 5% and 10% with SegFormer-B2 as the segmentation model to verify the effectiveness, respectively. We also execute the experiments of OnlySup and FullySup for reference, where OnlySup only uses the labeled data for training and FullySup uses all data. The experimental results are presented in Tables

TABLE V

COMPARISON RESULTS WITH SOTA METHODS ON ISPRS-POTS DAM DATASET. THE BEST RESULTS ARE HIGHLIGHTED IN BOLD. IOU, mIOU, mF1, AND KAPPA ARE REPRESENTED AS PERCENTAGES.

Ratio	Model	IoU					mIoU/mF1/Kappa
		Building	Low vegetation	Tree	Car	Impervious surfaces	
1%	OnlySup	69.80	59.39	59.50	66.50	55.85	62.21 / 76.58 / 0.6531
	Mean teacher [10]	72.53	58.98	60.43	67.97	67.39	65.46 / 79.01 / 0.7187
	CutMix [49]	55.58	42.05	49.72	50.86	39.40	47.52 / 64.21 / 0.5121
	CCT [38]	54.48	61.28	48.56	52.95	60.71	55.59 / 71.34 / 0.5761
	CPS [39]	59.35	69.16	62.89	59.88	66.33	63.52 / 77.63 / 0.6539
	LSST [50]	68.74	75.24	54.74	62.09	68.80	65.92 / 79.25 / 0.6847
	FixMatch [11]	76.95	71.59	64.71	65.85	72.81	70.38 / 82.53 / 0.7287
	UniMatch [18]	76.52	70.99	65.44	66.62	72.64	70.44 / 82.59 / 0.7291
	DWL [9]	72.34	77.08	62.74	62.57	72.22	69.39 / 81.79 / 0.7191
	AllSpark [12]	83.70	65.92	59.64	69.77	75.31	70.87 / 82.68 / 0.7827
	Our (MUCA)	84.56	66.98	56.96	71.52	76.64	71.33 / 82.92 / 0.7880
5%	OnlySup	84.22	64.10	60.81	74.04	76.88	72.01 / 83.10 / 0.7371
	Mean teacher [10]	82.15	65.92	67.11	72.21	74.60	72.40 / 83.86 / 0.7403
	CutMix [49]	52.94	68.86	41.51	58.33	54.82	55.29 / 70.79 / 0.5783
	CCT [38]	72.90	80.25	64.23	58.32	74.42	70.02 / 82.12 / 0.7236
	CPS [39]	76.53	84.34	57.98	69.45	75.39	72.74 / 83.78 / 0.7492
	LSST [50]	69.26	84.55	67.33	67.49	73.86	72.50 / 83.67 / 0.7399
	FixMatch [11]	78.12	74.87	68.89	66.58	75.30	72.75 / 84.15 / 0.7497
	UniMatch [18]	78.24	73.59	67.17	66.64	75.07	72.14 / 83.73 / 0.7432
	DWL [9]	74.81	85.64	66.38	62.99	75.68	73.10 / 84.22 / 0.7507
	AllSpark [12]	85.57	67.62	60.61	73.48	77.15	72.88 / 84.04 / 0.7989
	Our (MUCA)	88.45	69.53	61.39	74.18	79.56	74.62 / 85.15 / 0.8166
10%	OnlySup	83.01	69.26	66.83	75.02	75.47	73.92 / 84.89 / 0.7564
	Mean teacher [10]	84.76	69.28	68.83	71.66	76.51	74.21 / 85.07 / 0.7578
	CutMix [49]	64.55	80.99	64.79	65.50	68.01	68.77 / 81.34 / 0.7109
	CCT [38]	73.09	83.94	61.12	60.45	73.06	70.33 / 82.27 / 0.7265
	CPS [39]	77.80	87.15	61.12	68.48	75.89	74.09 / 84.55 / 0.7533
	LSST [50]	70.92	86.06	68.91	70.22	74.89	74.20 / 84.95 / 0.7549
	FixMatch [11]	77.97	76.17	70.09	70.97	76.14	74.27 / 85.20 / 0.7606
	UniMatch [18]	77.34	87.75	70.79	56.65	76.46	73.80 / 84.52 / 0.7599
	DWL [9]	76.37	88.42	66.54	64.37	77.14	74.57 / 85.16 / 0.7628
	AllSpark [12]	86.29	69.83	64.17	75.23	78.31	74.76 / 85.35 / 0.8144
	Our (MUCA)	88.02	70.58	64.53	75.20	79.92	75.65 / 85.90 / 0.8245
100%	FullySup	90.81	72.08	68.32	76.09	82.56	77.97 / 87.40 / 0.8459

V and VI, respectively. From the viewpoint of methods, our observations reveal the following trends. Methods such as CutMix and CCT exhibit a performance decline when incorporating unlabeled data into the training process, compared to the basic OnlySup method. In contrast, methods like FixMatch, UniMatch, DWL, and the proposed MUCA demonstrate a beneficial impact on performance. MUCA achieves the best results. There are many possible reasons. For example, methods like CutMix and CCT use all unlabeled data for consistency regularization during training without selective filtering. This may inadvertently result in memorizing a large number of incorrect pseudo-labels. On the other hand, FixMatch, UniMatch, DWL, and MUCA employ strategies such as careful

filtering or weighting of pseudo-labels in the unlabeled data, which reduces the harmful impact of low-confidence samples and prevents the dominance of most classes.

Additionally, an interesting phenomenon is that sometimes the performance of UniMatch is lower than that of FixMatch. UniMatch extends FixMatch by introducing an additional perturbation branch and a feature re-perturbation branch to enrich the representation space. Both branches are supervised by a weakly augmented branch. However, RS datasets often contain too many hard-to-distinguish classes and noise. They hinder the training process on the unlabeled data, which could be exacerbated by the inclusion of additional pseudo-supervision branches. In contrast, our method achieves better results by

TABLE VI
COMPARISON RESULTS WITH OTHER SOTA METHODS ON THE LOVE-DA DATASET. THE BEST RESULTS ARE IN BOLD. IOU, mIOU, mF1, AND KAPPA1 ARE REPRESENTED AS PERCENTAGES.

Ratio	Model	IoU							mIoU/mF1/Kappa
		Background	Building	Road	Water	Barren	Forest	Agriculture	
1%	OnlySup	41.96	37.86	36.74	57.03	9.02	31.70	37.73	36.01 / 51.41 / 0.4141
	Mean teacher [10]	44.73	42.53	40.34	50.92	11.37	26.88	54.40	38.73 / 52.81 / 0.4251
	CutMix [49]	36.04	24.69	10.03	24.60	3.43	6.67	10.19	16.52 / 26.85 / 0.1362
	CCT [38]	37.16	22.41	27.86	43.98	14.51	25.38	36.67	29.71 / 44.99 / 0.3517
	CPS [39]	46.52	20.87	27.85	50.55	0.01	33.16	34.60	30.51 / 44.28 / 0.3802
	LSST [50]	44.73	41.90	39.90	62.65	29.27	31.26	48.29	42.57 / 59.00 / 0.4817
	FixMatch [11]	46.78	51.20	50.21	67.27	11.53	36.79	50.26	44.86 / 60.02 / 0.5175
	UniMatch [18]	46.53	51.38	49.36	67.74	10.86	33.40	52.28	44.51 / 59.51 / 0.5175
	DWL [9]	48.74	56.79	51.59	63.42	22.56	35.20	55.38	47.67 / 63.40 / 0.5534
	AllSpark [12]	63.87	47.70	46.05	61.52	35.31	30.94	55.64	48.72 / 63.29 / 0.5502
	Our (MUCA)	64.89	56.03	47.14	63.86	35.81	22.57	58.18	49.78 / 63.48 / 0.5753
5%	OnlySup	48.00	43.34	50.56	61.42	23.14	37.63	45.00	44.20 / 60.46 / 0.5061
	Mean teacher [10]	49.73	46.22	42.34	60.93	31.51	35.79	44.22	44.39 / 61.81 / 0.5151
	CutMix [49]	41.48	41.62	38.77	47.44	14.69	28.09	31.05	34.73 / 50.65 / 0.3692
	CCT [38]	46.80	44.62	46.80	60.95	24.83	29.03	44.30	42.48 / 58.74 / 0.4850
	CPS [39]	48.90	49.64	47.97	60.27	4.67	36.09	47.32	42.12 / 56.90 / 0.4976
	LSST [50]	51.48	45.66	52.66	67.63	33.52	35.80	48.60	47.91 / 64.10 / 0.5434
	FixMatch [11]	45.40	53.05	51.22	66.73	28.53	27.25	54.30	44.64 / 62.45 / 0.5378
	UniMatch [18]	50.20	54.49	50.46	67.18	26.79	30.06	54.86	47.72 / 63.46 / 0.5543
	DWL [9]	48.75	55.00	51.53	69.49	29.46	36.59	52.11	48.99 / 64.88 / 0.5597
	AllSpark [12]	65.09	55.06	47.59	67.10	34.67	26.86	51.87	49.75 / 64.91 / 0.5682
	Our (MUCA)	67.29	56.04	48.37	61.02	36.21	30.76	57.09	50.97 / 64.92 / 0.5856
10%	OnlySup	47.02	51.04	50.73	59.42	31.66	38.25	51.26	47.05 / 63.52 / 0.5254
	Mean teacher [10]	50.45	55.75	43.56	66.15	35.24	36.96	45.64	47.68 / 64.18 / 0.5387
	CutMix [49]	46.73	49.60	47.36	59.99	29.06	37.77	40.60	44.44 / 60.99 / 0.4837
	CCT [38]	44.07	45.22	47.65	57.12	24.41	32.50	45.07	42.29 / 58.73 / 0.4762
	CPS [39]	51.30	54.93	52.57	53.37	18.39	37.59	53.24	45.91 / 61.78 / 0.5479
	LSST [50]	50.69	49.50	52.63	69.85	27.25	36.24	52.06	48.32 / 64.17 / 0.5565
	FixMatch [11]	52.02	55.59	53.20	57.91	25.86	40.83	57.50	48.99 / 64.97 / 0.5676
	UniMatch [18]	51.80	53.95	51.17	58.15	25.60	38.72	54.86	47.75 / 63.86 / 0.5639
	DWL [9]	49.94	56.66	53.89	70.35	30.62	41.49	53.13	50.87 / 66.64 / 0.5753
	AllSpark [12]	67.13	56.16	40.67	63.58	32.54	32.03	56.91	49.86 / 63.97 / 0.5751
	Our (MUCA)	68.69	58.20	41.82	65.62	37.09	35.01	57.38	51.97 / 66.72 / 0.5901
100%	FullySup	68.84	58.57	48.02	70.39	43.28	38.59	62.30	55.71 / 69.10 / 0.6291

using MSUC to exclude pseudo-labels with high uncertainty and utilizing CTSA to enhance the correlation WA and SA.

Furthermore, it is worth noting that our model outperforms all other SOTA methods on ISPRS-Potsdam and LoveDA datasets when the labeled data ratios are 1%, 5%, and 10%, respectively. This is a good demonstration of the fact that our semi-supervised model achieves better applicability on RS datasets with a very small labeled data ratio.

For specific classes, both datasets include categories that are difficult to distinguish. For example, the ISPRS-Potsdam dataset includes Building, Low vegetation, Tree, and Impervious surfaces, while the LoveDA dataset includes categories such as Building, Barren, Forest, and Agriculture. Our method, MUCA, achieves an improvement on IoU for almost all classes

compared to OnlySup when the labeled data ratios are 1%, 5%, and 10%. Additionally, when the labeled data ratios are 1%, 5%, and 10%, MUCA outperforms other SOTA models in *IoU* performance for the Building, Car, and Impervious surfaces classes in the ISPRS-Potsdam dataset, and for the Background, Building, Barren, and Agriculture classes in the LoveDA dataset. Although MUCA does not achieve the best *IoU* for all classes, this phenomenon is understandable and explainable. This is because different algorithms have different focuses, which make one algorithm perform exceptionally well on specific classes while underperforming for others. However, focusing solely on improving a single class is not the research focus of this paper. For example, while the DWL model achieves significant improvement in the Low vegetation class,

TABLE VII
MODEL GENERALIZABILITY EXPERIMENTS.

Network	Model	mIoU(5%)
U-Net	Onlysup	57.52
	NoUC	61.59
	MUCA	64.21
PSPNet	Onlysup	63.46
	NoUC	66.16
	MUCA	68.87
DeepLabv3+	Onlysup	66.83
	NoUC	68.01
	MUCA	70.49
SegFormer-B2	Onlysup	72.01
	NoUC	73.14
	MUCA	74.62

its performance on the Building, Car, and Impervious surfaces classes is unsatisfactory.

F. Model generalizability experiments

The proposed model is non-intrusive and can be easily integrated into existing semantic segmentation networks without changing the network structure itself. Therefore, we conduct experiments by integrating our model into several popular networks including U-Net, PSPNet, DeepLabv3+, and SegFormer-B2 on ISPRS-Potsdam dataset. These experiments are designed to evaluate the general applicability of the MUCA on segmentation models. The first three of these models are classical CNN semantic segmentation models, and the last one is based on the Transformer architecture. We comparative analyze the performance improvement of MUCA with Onlysup and NoUC on these models. NoUC, as clearly defined in the Ablation Study section, refers to a simplified method that does not perform uncertainty estimation or incorporate the CTSA module. Instead, it relies solely on standard consistency regularization to calculate the loss of feature maps at each layer. The model general applicability experiments were performed on 5% labeled training data and the results are shown in Table VII.

It can be seen that semi-supervised model MUCA achieves significant improvements with 5% labeled training data. It enhances the performance of popular semantic segmentation models including U-Net, PSPNet, DeepLabv3+, and SegFormer-B2. This shows that our MUCA has the ability to improve the performance of classical CNN-based semantic segmentation models and novel Transformer architecture models.

G. Visualization Comparison

We conducted visual comparison experiments to see the advantages of our approach more intuitively and clearly. Fig. 6 shows the visual comparison of several semi-supervised semantic segmentation methods on the ISPRS-Potsdam dataset.

The Fixmatch and Unimatch make errors in segmenting regions for the Low vegetation, Tree, Impervious surfaces and Building classes. Allspark successfully recognizes part of the region where Low vegetation classes are mixed with Tree classes, but the segmentation results are significantly enlarged for building classes. In contrast, our method shows significant advantages in accurately recognizing and segmenting Building (blue), Car (yellow), and Tree (green). Especially, we can see that methods including Fixmatch and Unimatch show large-scale segmentation errors when Car, Low vegetation and Tree are mixed. In addition, we overlap our segmentation results with the original image in the last column to clearly show our advantage. This overlapped image demonstrates that our model achieves excellent visual results, particularly in the Tree and Car categories.

V. DISCUSSION AND CONCLUSION

Our study addresses the challenges associated with semi-supervised RS image semantic segmentation by proposing the Multi-Scale Uncertainty and Cross-Teacher-Student Attention (MUCA) model. The MUCA model includes two special modules, i.e., Multi-scale Uncertainty Consistency (MSUC) and Cross-Teacher-Student Attention (CTSA). The goal of MSUC is to learn rich multi-scale information, meanwhile, CTSA distinguishes the high inter-class similarities through the cross-network attention mechanism. The new features constructed by CTSA enable the student network decoder to benefit from the dual enhancement of both WA and SA, achieving better optimization results and demonstrating greater stability during the training phase.

Compared to SOTA algorithms, our method achieved the best results for the metrics $mIoU$, $mF1$, and $Kappa$, however, did not achieve the best IoU for all the categories. This phenomenon is understandable and explainable. On the one hand, this paper does not address other problems in the semi-supervised domain such as long-tailed distribution among classes. On the other hand, different algorithms have different focuses which may lead to a particularly good result for one class and a poor result for others. This study highlights the more realistic scenario where MUCA demonstrates the best overall performance across all classes. Finally, we hope that the model proposed in this paper can serve as a simple and powerful baseline in the field of semi-supervised semantic segmentation of RS images. We also aim to inspire more valuable research for future work.

REFERENCES

- [1] X. He, Y. Zhou, J. Zhao, D. Zhang, R. Yao, and Y. Xue, "Swin transformer embedding unet for remote sensing image semantic segmentation," *IEEE Transactions on Geoscience and Remote Sensing*, vol. 60, pp. 1–15, 2022.
- [2] D. Hong, B. Zhang, X. Li, Y. Li, C. Li, J. Yao, N. Yokoya, H. Li, P. Ghamisi, X. Jia *et al.*, "Spectralgpt: Spectral remote sensing foundation model," *IEEE Transactions on Pattern Analysis and Machine Intelligence*, 2024.
- [3] X. Sun, M. Zhang, J. Dong, R. Lguensat, Y. Yang, and X. Lu, "A deep framework for eddy detection and tracking from satellite sea surface height data," *IEEE Transactions on Geoscience and Remote Sensing*, vol. 59, no. 9, pp. 7224–7234, 2020.

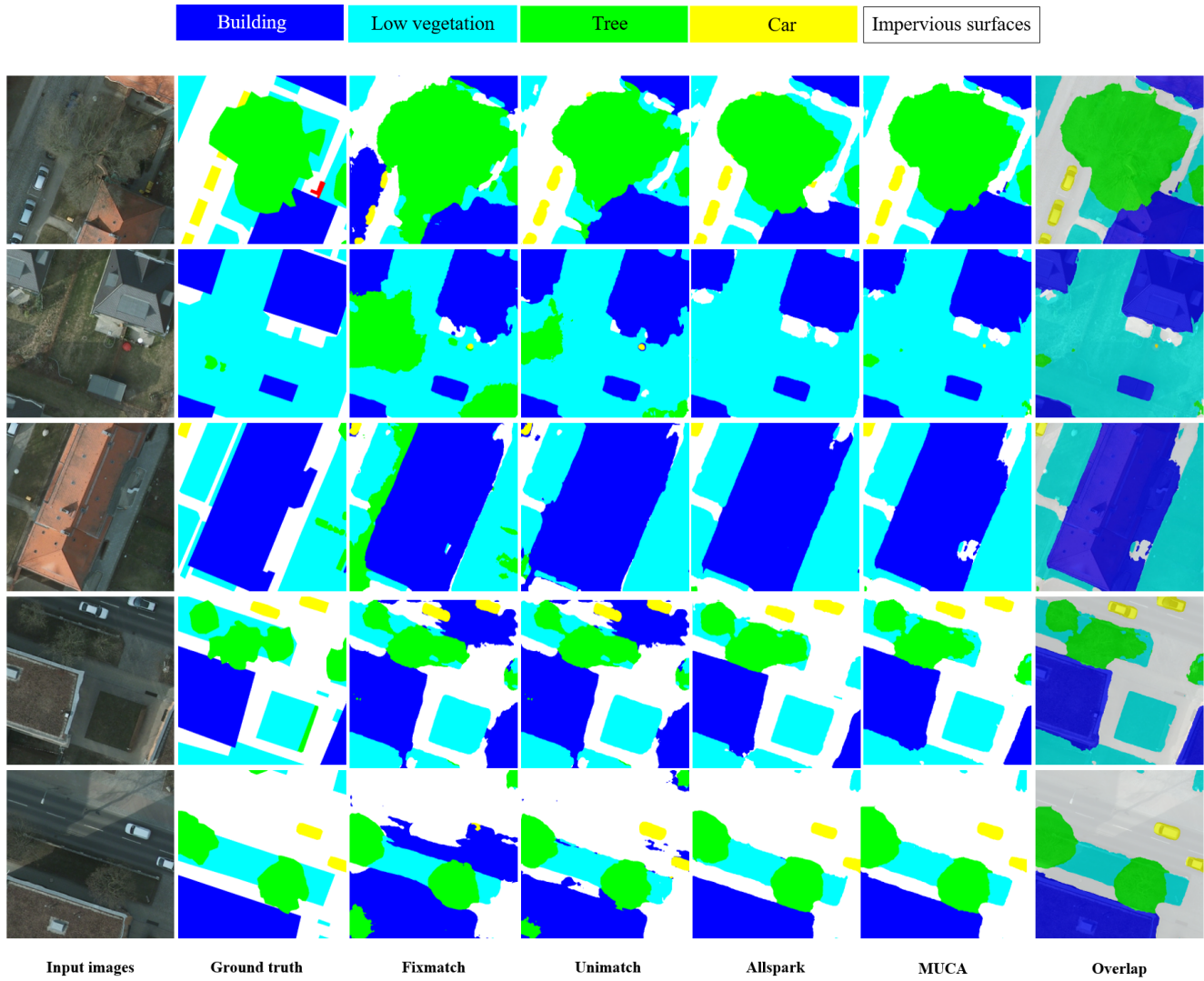


Fig. 6. Visual comparison of semantic segmentation results with different semisupervised methods on the ISPRS-Potsdam dataset.

- [4] C. Xu, X. Du, X. Fan, Z. Yan, X. Kang, J. Zhu, and Z. Hu, "A modular remote sensing big data framework," *IEEE Transactions on Geoscience and Remote Sensing*, vol. 60, pp. 1–11, 2021.
- [5] Y. Yang, X. Sun, J. Dong, K.-M. Lam, and X. Xiang Zhu, "Attention-convnet network for ocean-front prediction via remote sensing sst images," *IEEE Transactions on Geoscience and Remote Sensing*, vol. 62, pp. 1–16, 2024.
- [6] X. X. Zhu, D. Tuia, L. Mou, G.-S. Xia, L. Zhang, F. Xu, and F. Fraundorfer, "Deep learning in remote sensing: A comprehensive review and list of resources," *IEEE geoscience and remote sensing magazine*, vol. 5, no. 4, pp. 8–36, 2017.
- [7] D. Wen, X. Huang, F. Bovolo, J. Li, X. Ke, A. Zhang, and J. A. Benediktsson, "Change detection from very-high-spatial-resolution optical remote sensing images: Methods, applications, and future directions," *IEEE Geoscience and Remote Sensing Magazine*, vol. 9, no. 4, pp. 68–101, 2021.
- [8] Y. Xin, Z. Fan, X. Qi, Y. Zhang, and X. Li, "Confidence-weighted dual-teacher networks with biased contrastive learning for semi-supervised semantic segmentation in remote sensing images," *IEEE Transactions on Geoscience and Remote Sensing*, 2024.
- [9] W. Huang, Y. Shi, Z. Xiong, and X. X. Zhu, "Decouple and weight semi-supervised semantic segmentation of remote sensing images," *ISPRS Journal of Photogrammetry and Remote Sensing*, vol. 212, pp. 13–26, 2024.
- [10] A. Tarvainen and H. Valpola, "Mean teachers are better role models: Weight-averaged consistency targets improve semi-supervised deep learning results," *Advances in neural information processing systems*, vol. 30, 2017.
- [11] K. Sohn, D. Berthelot, N. Carlini, Z. Zhang, H. Zhang, C. A. Raffel, E. D. Cubuk, A. Kurakin, and C.-L. Li, "Fixmatch: Simplifying semi-supervised learning with consistency and confidence," *Advances in neural information processing systems*, vol. 33, pp. 596–608, 2020.
- [12] H. Wang, Q. Zhang, Y. Li, and X. Li, "Allspark: Reborn labeled features from unlabeled in transformer for semi-supervised semantic segmentation," in *Proceedings of the IEEE/CVF Conference on Computer Vision and Pattern Recognition (CVPR)*, June 2024, pp. 3627–3636.
- [13] A. Peláez-Vegas, P. Mesejo, and J. Luengo, "A survey on semi-supervised semantic segmentation," *arXiv preprint arXiv:2302.09899*, 2023.
- [14] F. Zhang, Y. Shi, Z. Xiong, W. Huang, and X. X. Zhu, "Pseudo features-guided self-training for domain adaptive semantic segmentation of satellite images," *IEEE Transactions on Geoscience and Remote Sensing*, vol. 61, pp. 1–14, 2023.
- [15] J. Jin, W. Lu, H. Yu, X. Rong, X. Sun, and Y. Wu, "Dynamic and adaptive self-training for semi-supervised remote sensing image semantic segmentation," *IEEE Transactions on Geoscience and Remote Sensing*, 2024.
- [16] X. Cai, Q. Lai, Y. Wang, W. Wang, Z. Sun, and Y. Yao, "Poly kernel inception network for remote sensing detection," in *Proceedings of the IEEE/CVF Conference on Computer Vision and Pattern Recognition*, 2024, pp. 27706–27716.
- [17] L. Zhang and L. Zhang, "Artificial intelligence for remote sensing data

- analysis: A review of challenges and opportunities,” *IEEE Geoscience and Remote Sensing Magazine*, vol. 10, no. 2, pp. 270–294, 2022.
- [18] L. Yang, L. Qi, L. Feng, W. Zhang, and Y. Shi, “Revisiting weak-to-strong consistency in semi-supervised semantic segmentation,” in *Proceedings of the IEEE/CVF Conference on Computer Vision and Pattern Recognition*, 2023, pp. 7236–7246.
 - [19] X. Sun, C. Chen, X. Wang, J. Dong, H. Zhou, and S. Chen, “Gaussian dynamic convolution for efficient single-image segmentation,” *IEEE Transactions on Circuits and Systems for Video Technology*, vol. 32, no. 5, pp. 2937–2948, 2021.
 - [20] F. Zhou, X. Sun, C. Sun, J. Dong, and X. X. Zhu, “Adaptive morphology filter: A lightweight module for deep hyperspectral image classification,” *IEEE Transactions on Geoscience and Remote Sensing*, vol. 61, pp. 1–16, 2023.
 - [21] Z. Xiong, F. Zhang, Y. Wang, Y. Shi, and X. X. Zhu, “Earthnets: Empowering artificial intelligence for earth observation,” *IEEE Geoscience and Remote Sensing Magazine*, 2024.
 - [22] X. Li, C. Wen, Y. Hu, Z. Yuan, and X. X. Zhu, “Vision-language models in remote sensing: Current progress and future trends,” *IEEE Geoscience and Remote Sensing Magazine*, 2024.
 - [23] D. Hong, B. Zhang, H. Li, Y. Li, J. Yao, C. Li, M. Werner, J. Chanussot, A. Zipf, and X. X. Zhu, “Cross-city matters: A multimodal remote sensing benchmark dataset for cross-city semantic segmentation using high-resolution domain adaptation networks,” *Remote Sensing of Environment*, vol. 299, p. 113856, 2023.
 - [24] R. Deng, Z. Guo, Q. Chen, X. Sun, Q. Chen, H. Wang, and X. Liu, “A dual spatial-graph refinement network for building extraction from aerial images,” *IEEE Transactions on Geoscience and Remote Sensing*, 2023.
 - [25] G. Zhou, W. Liu, Q. Zhu, Y. Lu, and Y. Liu, “Eca-mobilenetv3 (large)+ segnet model for binary sugarcane classification of remotely sensed images,” *IEEE Transactions on Geoscience and Remote Sensing*, vol. 60, pp. 1–15, 2022.
 - [26] X. Wu, D. Hong, and J. Chanussot, “Uiu-net: U-net in u-net for infrared small object detection,” *IEEE Transactions on Image Processing*, vol. 32, pp. 364–376, 2022.
 - [27] X. Wang, B. Zhang, L. Yu, and J. Xiao, “Hunting sparsity: Density-guided contrastive learning for semi-supervised semantic segmentation,” in *Proceedings of the IEEE/CVF Conference on Computer Vision and Pattern Recognition*, 2023, pp. 3114–3123.
 - [28] S. Workman, A. Hadzic, and M. U. Rafique, “Handling image and label resolution mismatch in remote sensing,” in *Proceedings of the IEEE/CVF Winter Conference on Applications of Computer Vision*, 2023, pp. 3709–3718.
 - [29] Y. Quan, A. Yu, X. Cao, C. Qiu, X. Zhang, B. Liu, and P. He, “Building extraction from remote sensing images with dog as prior constraint,” *IEEE Journal of Selected Topics in Applied Earth Observations and Remote Sensing*, vol. 15, pp. 6559–6570, 2022.
 - [30] J. Li, J. Zhang, J. Han, C. Yan, and D. Zeng, “Progressive recurrent neural network for multispectral remote sensing image destriping,” *IEEE Transactions on Geoscience and Remote Sensing*, 2023.
 - [31] H.-F. Zhong, Q. Sun, H.-M. Sun, and R.-S. Jia, “Nt-net: A semantic segmentation network for extracting lake water bodies from optical remote sensing images based on transformer,” *IEEE Transactions on Geoscience and Remote Sensing*, vol. 60, pp. 1–13, 2022.
 - [32] Y. Du, Y. Shen, H. Wang, J. Fei, W. Li, L. Wu, R. Zhao, Z. Fu, and Q. Liu, “Learning from future: A novel self-training framework for semantic segmentation,” *Advances in Neural Information Processing Systems*, vol. 35, pp. 4749–4761, 2022.
 - [33] R. Ke, A. I. Aviles-Rivero, S. Pandey, S. Reddy, and C.-B. Schönlieb, “A three-stage self-training framework for semi-supervised semantic segmentation,” *IEEE Transactions on Image Processing*, vol. 31, pp. 1805–1815, 2022.
 - [34] J. Yuan, Y. Liu, C. Shen, Z. Wang, and H. Li, “A simple baseline for semi-supervised semantic segmentation with strong data augmentation,” in *Proceedings of the IEEE/CVF International Conference on Computer Vision*, 2021, pp. 8229–8238.
 - [35] Y. Jin, J. Wang, and D. Lin, “Semi-supervised semantic segmentation via gentle teaching assistant,” *Advances in Neural Information Processing Systems*, vol. 35, pp. 2803–2816, 2022.
 - [36] Y. Wang, H. Wang, Y. Shen, J. Fei, W. Li, G. Jin, L. Wu, R. Zhao, and X. Le, “Semi-supervised semantic segmentation using unreliable pseudo-labels,” in *Proceedings of the IEEE/CVF conference on computer vision and pattern recognition*, 2022, pp. 4248–4257.
 - [37] V. Olsson, W. Tranheden, J. Pinto, and L. Svensson, “Classmix: Segmentation-based data augmentation for semi-supervised learning,” in *Proceedings of the IEEE/CVF winter conference on applications of computer vision*, 2021, pp. 1369–1378.
 - [38] Y. Ouaili, C. Hudelot, and M. Tami, “Semi-supervised semantic segmentation with cross-consistency training,” in *Proceedings of the IEEE/CVF conference on computer vision and pattern recognition*, 2020, pp. 12674–12684.
 - [39] X. Chen, Y. Yuan, G. Zeng, and J. Wang, “Semi-supervised semantic segmentation with cross pseudo supervision,” in *Proceedings of the IEEE/CVF conference on computer vision and pattern recognition*, 2021, pp. 2613–2622.
 - [40] B. Fang, Y. Li, H. Zhang, and J. C.-W. Chan, “Collaborative learning of lightweight convolutional neural network and deep clustering for hyperspectral image semi-supervised classification with limited training samples,” *ISPRS Journal of Photogrammetry and Remote Sensing*, vol. 161, pp. 164–178, 2020.
 - [41] L. Wang, M. Zhang, and W. Shi, “Stcnet: A semi-supervised network based on self-training and consistency regularization for change detection in vhr remote sensing images,” *IEEE Journal of Selected Topics in Applied Earth Observations and Remote Sensing*, 2023.
 - [42] M. Cai, H. Chen, T. Zhang, Y. Zhuang, and L. Chen, “Consistency regularization based on masked image modeling for semi-supervised remote sensing semantic segmentation,” *IEEE Journal of Selected Topics in Applied Earth Observations and Remote Sensing*, 2024.
 - [43] W. Xuan, H. Qi, and A. Xiao, “Tsg-seg: Temporal-selective guidance for semi-supervised semantic segmentation of 3d lidar point clouds,” *ISPRS Journal of Photogrammetry and Remote Sensing*, vol. 216, pp. 217–228, 2024.
 - [44] G. Li, W. Liu, Q. Gao, Q. Wang, J. Han, and X. Gao, “Self-supervised edge perceptual learning framework for high-resolution remote sensing images classification,” *IEEE Transactions on Circuits and Systems for Video Technology*, 2023.
 - [45] Y. Gal and Z. Ghahramani, “Dropout as a bayesian approximation: Representing model uncertainty in deep learning,” in *international conference on machine learning*. PMLR, 2016, pp. 1050–1059.
 - [46] O. Chapelle, B. Scholkopf, and A. Zien, “Semi-supervised learning (chapelle, o. et al., eds.; 2006)[book reviews],” *IEEE Transactions on Neural Networks*, vol. 20, no. 3, pp. 542–542, 2009.
 - [47] J. Wang, Z. Zheng, A. Ma, X. Lu, and Y. Zhong, “Loveda: A remote sensing land-cover dataset for domain adaptive semantic segmentation,” in *Proceedings of the Neural Information Processing Systems Track on Datasets and Benchmarks*, J. Vanschoren and S. Yeung, Eds., vol. 1. Curran Associates, Inc., 2021.
 - [48] ISPRS, “ISPRS Potsdam Dataset,” https://www.isprs.org/education/benchmarks/UrbanSemLab/2d-sem-label-potsdam.aspx?utm_source=chatgpt.com, 2018, accessed: 2024-10-8.
 - [49] S. Yun, D. Han, S. J. Oh, S. Chun, J. Choe, and Y. Yoo, “Cutmix: Regularization strategy to train strong classifiers with localizable features,” in *Proceedings of the IEEE/CVF international conference on computer vision*, 2019, pp. 6023–6032.
 - [50] X. Lu, L. Jiao, F. Liu, S. Yang, X. Liu, Z. Feng, L. Li, and P. Chen, “Simple and efficient: A semisupervised learning framework for remote sensing image semantic segmentation,” *IEEE Transactions on Geoscience and Remote Sensing*, vol. 60, pp. 1–16, 2022.